Cooperative Localisation of a GPS-Denied UAV using Direction-of-Arrival Measurements

James S. Russell, Mengbin Ye, Brian D.O. Anderson, Hatem Hmam, Peter Sarunic

***Abstract*—A GPS-denied UAV (Agent B) is localised through INS alignment with the aid of a nearby GPS-equipped UAV (Agent A), which broadcasts its position at several time instants. Agent B measures the signals' direction of arrival with respect to Agent B's inertial navigation frame. Semidefinite programming and the Orthogonal Procrustes algorithm are employed, and accuracy is improved through maximum likelihood estimation. The method is validated using flight data and simulations. A three-agent extension is explored.**

***Index Terms*—Localisation, INS alignment, Direction-of-Arrival Measurement, GPS-Denied, Semidefinite Programming**

I. Introduction

Unmanned aerial vehicles (UAVs) play a central role in many defence reconnaissance and surveillance operations. Formations of UAVs can provide greater reliability and coverage when compared to a single UAV. To provide meaningful data in such operations, all UAVs in a formation must have a common reference frame (typically the global frame). Traditionally, UAVs have access to the global frame via GPS. However, GPS signals may be lost in urban environments and enemy controlled airspace (jamming). Overcoming loss of GPS signal is a hot topic in research [1], and offers a range of different problems in literature [2], [3].

Without access to global coordinates, a UAV must rely on its inertial navigation system (INS). Stochastic error in on-board sensor measurements causes the INS frame to accumulate drift. At any given time, drift can be characterised by a rotation and translation with respect to the global frame, and is assumed to be independent between UAVs in a formation. INS frame drift therefore cannot be modelled deterministically. Information from global and INS frames must be collected in order to determine the drift between frames and align the INS frame with the global frame. We describe this process as cooperative localisation when multiple vehicles interact for this purpose.

Signals of opportunity (SOP) such as AM/FM radio, digital television or cellular communication can serve as references to assist in characterizing the misalignment between navigation frames of multiple agents. Recent contributions in this field include [4]–[6]. In contexts where SOP are either unavailable or unreliable, various measurement types such as distance between agents and direction of arrival of a signal (we henceforth call DOA[1]) can be used for this process. In the context of UAVs, additional sensors add weight and consume power. As a result, one generally aims to minimise the number of measurement types required for localisation. This paper studies a cooperative approach to localisation using DOA measurements.

When two or more GPS-enabled UAVs can simultaneously measure directions *with respect to the global frame* towards the GPS-denied UAV, the location of the GPS-denied UAV is given by the point minimising distances to the half-line loci derived from the directional measurements [7]–[9]. Operational requirements may limit the number of nearby GPS-enabled UAVs to one single agent. We therefore seek a solution which does not require simultaneous measurements to a single point.

When the GPS-denied agent is able to simultaneously measure directions *with respect to its local INS frame* towards multiple landmarks with known global coordinates, triangulation-based measurements can be used to achieve localisation. This problem is studied in three-dimensional space in [10], and in two-dimensional space in [11], [12]. If only one landmark bearing can be measured at any given time, a bearing-only SLAM algorithm may be used to progressively construct a map of the environment on the condition each landmark is seen at least twice. Alignment of a GPS-denied agent's INS frame could then be achieved by determining the rotation and translation between the map's coordinate frame and the global coordinate frame. In practice, landmark locations may be unknown, or there may be no guarantee they are stationary or permanent, and hence we require a localisation algorithm which is independent of landmarks in the environment. Iterative filtering methods such as the Extended Kalman Filter (EKF) are often required when drift is significant between updates. In [13], an EKF is used to estimate drift in the context of marine localisation. In our problem context the drift is sufficiently slow to be modelled as stationary over short periods. We are motivated to formulate a localisation algorithm which does not involve an iterative filtering technique.

Without reliance on landmarks, the only directional measurements available are between the GPS-denied and the GPS-enabled UAVs. Given the small size of their airframes with respect to their separation distance, these UAVs are

The work of Russell, Ye, and Anderson was supported by the Australian Research Council (ARC) Discovery Project DP-160104500, by 111-Project No. D17019, and by Data61-CSIRO. Ye was supported by an Australian Government Research Training Program (RTP) Scholarship.

J.S. Russell, M. Ye and B.D.O. Anderson are with the Research School of Engineering, Australian National University, Canberra, Australia {u5542624, mengbin.ye, brian.anderson}@anu.edu.au. B.D.O. Anderson is also with Hangzhou Dianzi University, Hangzhou, China, and with Data61-CSIRO in Canberra, Australia. H. Hmam and P. Sarunic are with Australian Defence Science and Technology Group (DST Group), Edinburgh, Australia {hatem.hmam, peter.sarunic}@dst.defence.gov.au.

[1]A bearing generally describes a scalar measurement between two points in a plane, whereas a direction-of-arrival is a vector measurement between two points in three-dimensional ambient space (as considered in this paper).

modelled as point agents, and therefore one single directional measurement is available at any given time. A stationary target is localised by an agent using bearing-only measurements in two-dimensional space [14], [15], and in three-dimensional space [16]. A similar problem is considered in [17], in which a mobile source is localised using measurements received at a stationary receiver using an iterative filtering technique. However, for operational reasons, the agent requiring localisation may be unable to broadcast signals, or agents involved may not be allowed to remain stationary. In such instances, the approaches in [14]–[17] are not suitable. Commonly used computer vision techniques such as structure from motion [18] require directional measurements towards multiple stationary points or towards a stationary point from multiple known positions. This is not possible in our problem context. The measurement and motion requirements we are imposing therefore represent a significant technical challenge. One algorithm satisfying all the requirements above was proposed in [19], in which two agents perform sinusoidal motion in two-dimensional ambient space. Directional measurements are used to obtain the distance between Agents A and B, but localisation of B in the global frame is not achieved.

Motivated by interest from Australia's Defence Science and Technology Group, this paper seeks to address the problem of localising a GPS-denied UAV with the assistance of a GPS-enabled UAV, which we will call Agent B and A respectively. Both agents move arbitrarily in three-dimensional space. Agent B navigates using an INS frame. Agent A broadcasts its position in the global coordinate frame at discrete instants in time. For each broadcast, Agent B is able to take a DOA measurement towards Agent A.

The problem setup and the solution we propose are both novel. In particular, while the literature discussed above considers certain aspects from the following list, none consider all of the following aspects simultaneously:

- The network consists of only two mobile agents (and is therefore different to the sensor network localisation problems in the literature).
- There is no a priori knowledge or sensing of a stationary reference point in the global frame.
- Both UAVs are free to execute arbitrary motion in three-dimensional space, with the exception of a small number of geometrically unsolvable trajectory pairs[2].
- Cooperation occurs through *unidirectional* signal transmission. Agent A broadcasts its global position (acquired using GPS) to Agent B (which is GPS-denied).

When performing non-routine operations in unfamiliar environments, any combination of these four aspects may be required with short notice. As a result, we are motivated to determine a reliable general solution to the cooperative localisation problem.

In [20], this problem is studied in two-dimensional space using bearing measurements, but the added (third) dimension in our paper means 2 scalar quantities, not 1, are obtained per measurement. This significantly complicates the problem, thus requiring new techniques to be introduced.

In our proposed solution, we localise Agent B by identifying the relationship between the global frame (navigated by Agent A) and the inertial navigation frame of Agent B. The relationship is identified by solving a system of linear equations for a set of unknown variables. The nature of the problem means quadratic constraints exist on some of the variables. To improve robustness against noisy measurements, we exploit the quadratic constraints and use semidefinite programming (SDP) and the Orthogonal Procrustes algorithm to obtain an initial solution for maximum likelihood (ML) estimation; this combined approach is a key novel contribution of this paper.

We evaluate the performance of the algorithm by (i) using a real set of trajectories and (ii) using Monte Carlo simulations. Sets of unsuitable trajectories are identified, in which our proposed method cannot feasibly obtain a unique solution. Finally, we explore an extension of the algorithm to a three-agent network in which two agents are GPS-denied.

The rest of the paper is structured as follows. In Section II the problem is formalised. In Section III a localisation method using a linear equation formulation is proposed. Section IV extends this method to semidefinite programming to produce a more robust localisation algorithm. In Section V, a maximum likelihood estimation method is presented to refine results further. Section VI presents simulation results to evaluate the performance of the combined localisation algorithm. Section VII extends the localisation algorithm to a three-agent network. The paper is concluded in Section VIII. [3]

II. Problem Definition

Two agents, which we call Agent A and Agent B, travel along arbitrary trajectories in three-dimensional space. Agent A has GPS and therefore navigates with respect to the global frame. Because Agent B cannot access GPS, it has no ability to self-localise in the global frame, but can self-localise and navigate in a local inertial frame by integrating gyroscope and accelerometer measurements.

This two-agent localisation problem involves 4 frames as in Figure 1. The importance of each frame, and its use in obtaining the localisation, will be made clear in the sequel. Frames are labelled as follows:

- The global frame is A_1 (available only to Agent A),
- the local INS frame of Agent B is denoted by B_2,
- the body-centred INS frame of Agent B (axes of frames B_2 and B_3 are parallel by definition)is denoted B_3,
- the body-fixed frame of Agent B is denoted B_4.

The expression of directional measurements with respect to the INS frame in vector form motivates the definition of the body-centred frame B_3. Later, we find that differences in

[2]No constraints exist on the trajectories other than the physical limitations of the aircraft. See Section VI-C for further details on unsuitable trajectories.

[3]Early sections in this paper (covering up to and including employment of Orthogonal Procrustes algorithm) appeared in less detail in the conference paper [21]. Additions have been made to these sections - the literature review is now more extensive, and the role of different coordinate frames is much more explicitly set out; the algorithm's performance is now validated on real flight trajectories. Analysis of unsuitable trajectories, ML refinement and the three-agent extension are further extensions beyond [21].

body-fixed frame azimuth and elevation measurement noise motivate the use of B_4 for maximum likelihood estimation.

Note that agents A and B are denoted by a single letter, whereas frames A_1 and B_i for i = 2,3,4 are denoted by a letter-number pair. Let $\boldsymbol{p}_{\boldsymbol{J}}^{\boldsymbol{I_0}}(k)$ denote the position of Agent J in coordinates of frame I_0 at the k^{th} time instant. Let u_J, v_J, w_J denote Agent J's coordinates in the global frame (A_1), and x_J, y_J, z_J denote Agent J's coordinates in Agent B's local INS frame (B_2). It follows that:

$$\boldsymbol{p}_{\boldsymbol{A}}^{\boldsymbol{A_1}}(k) = [u_A(k),\ v_A(k),\ w_A(k)]^\top \tag{1}$$

$$\boldsymbol{p}_{\boldsymbol{B}}^{\boldsymbol{B_2}}(k) = [x_B(k),\ y_B(k),\ z_B(k)]^\top \tag{2}$$

The rotation and translation of Agent B's local INS frame (B_2) with respect to the global frame (A_1) evolves via drift. Although this drift is significant over long periods, frame B_2 can be modelled as stationary with respect to frame A_1 over short intervals[4]. During these short intervals, the following measurement process occurs multiple times. At each time instant k, the following four activities occur simultaneously :

- Agent B records its own position in the INS frame $\boldsymbol{p}_{\boldsymbol{B}}^{\boldsymbol{B_2}}(k)$.
- Agent A records and broadcasts its position in the global frame $\boldsymbol{p}_{\boldsymbol{A}}^{\boldsymbol{A_1}}(k)$.
- Agent B receives the broadcast of $\boldsymbol{p}_{\boldsymbol{A}}^{\boldsymbol{A_1}}(k)$ from Agent A, and measures this signal's DOA using instruments fixed to the UAV's fuselage. This directional measurement is therefore naturally referenced to the body-fixed frame B_4.
- Agent B's attitude, i.e. orientation with respect to the INS frames B_2 and B_3 is known. An expression for the DOA measurement referenced to the axes INS frames B_3 can therefore be easily calculated.

A DOA measurement, referenced to a frame with axes denoted x, y, z, is expressed as follows:

- Azimuth (θ): angle formed between the positive x axis and the projection of the free vector from Agent B towards Agent A onto the xy plane.
- Elevation (ϕ): angle formed between the free vector from Agent B towards Agent A and xy plane. The angle is positive if the z component of the unit vector towards Agent A is positive.

[4]If loss of GPS is sustained for extensive periods we recommend using the algorithm in this paper as an initialisation for a recursive filtering algorithm.

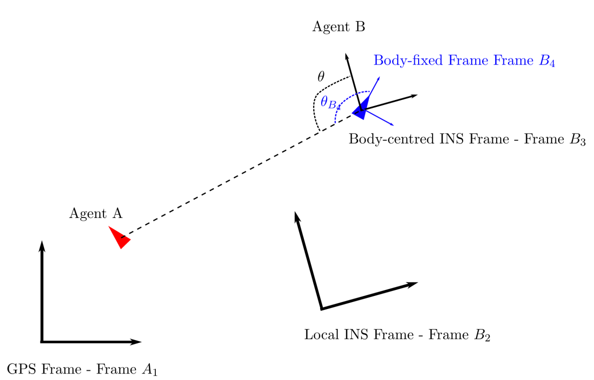

Fig. 1. Illustration of coordinate frames in a two-dimensional space

The problem addressed in this paper, namely the localisation of Agent B, is achieved if we can determine the relationship between the global frame A_1 and the local INS frame B_2. This information can be used to determine global coordinates of Agent B at each time instant k:

$$\boldsymbol{p}_{\boldsymbol{B}}^{\boldsymbol{A_1}}(k) = [u_B(k),\ v_B(k),\ w_B(k)]^\top \tag{3}$$

Passing between the global frame (A_1) and the local INS frame of Agent B (B_2) is achieved by a rotation of frame axes (defined by a rotation matrix, call it $\boldsymbol{R}_{\boldsymbol{A_1}}^{\boldsymbol{B_2}}$) and translation $\boldsymbol{t}_{\boldsymbol{A_1}}^{\boldsymbol{B_2}}$ of frame. For instance, the coordinate vector of the position of Agent A referenced to the INS frame of Agent B is:

$$\boldsymbol{p}_{\boldsymbol{A}}^{\boldsymbol{B_2}}(k) = \boldsymbol{R}_{\boldsymbol{A_1}}^{\boldsymbol{B_2}}\,\boldsymbol{p}_{\boldsymbol{A}}^{\boldsymbol{A_1}}(k) + \boldsymbol{t}_{\boldsymbol{A_1}}^{\boldsymbol{B_2}} \tag{4}$$

We therefore have

$$\boldsymbol{p}_{\boldsymbol{B}}^{\boldsymbol{A_1}}(k) = \boldsymbol{R}_{\boldsymbol{A_1}}^{\boldsymbol{B_2}\top}\,(\boldsymbol{p}_{\boldsymbol{B}}^{\boldsymbol{B_2}}(k) - \boldsymbol{t}_{\boldsymbol{A_1}}^{\boldsymbol{B_2}}) \tag{5}$$

where $\boldsymbol{R}_{\boldsymbol{A_1}}^{\boldsymbol{B_2}\top} = \boldsymbol{R}_{\boldsymbol{B_2}}^{\boldsymbol{A_1}}$ and $-\boldsymbol{R}_{\boldsymbol{A_1}}^{\boldsymbol{B_2}\top}\boldsymbol{t}_{\boldsymbol{A_1}}^{\boldsymbol{B_2}} = \boldsymbol{t}_{\boldsymbol{B_2}}^{\boldsymbol{A2}}$. The localisation problem can be reduced to solving for $\boldsymbol{R}_{\boldsymbol{A_1}}^{\boldsymbol{B_2}} \in SO(3)$ with entries r_{ij} and $\boldsymbol{t}_{\boldsymbol{A_1}}^{\boldsymbol{B_2}} \in \mathbb{R}^3$ with entries t_i.

The matrix $\boldsymbol{R}_{\boldsymbol{A_1}}^{\boldsymbol{B_2}}$ is a rotation matrix if and only if $\boldsymbol{R}_{\boldsymbol{A_1}}^{\boldsymbol{B_2}}\boldsymbol{R}_{\boldsymbol{A_1}}^{\boldsymbol{B_2}\top} = I_3$ and $\det(\boldsymbol{R}_{\boldsymbol{A_1}}^{\boldsymbol{B_2}}) = 1$. As will be seen in the sequel, these constraints are equivalent to a set of quadratic constraints on the entries of $\boldsymbol{R}_{\boldsymbol{A_1}}^{\boldsymbol{B_2}}$. In total there are 12 entries of $\boldsymbol{R}_{\boldsymbol{A_1}}^{\boldsymbol{B_2}}$ and $\boldsymbol{t}_{\boldsymbol{A_1}}^{\boldsymbol{B_2}}$ to be found as we work directly with r_{ij}.

III. Linear System Method

This section presents a linear system (LS) method to solving the localisation problem. Given enough measurements, the linear system approach can achieve exact localisation when using noiseless DOA measurements, so long as Agents A and B avoid a set of unsuitable trajectories (which are detailed in Section VI-C) in which rank-deficiency is encountered. Building on this, Section IV introduces non-linear constraints to the linear problem defined in this section to improve accuracy in the presence of noise.

A. Forming a system of linear equations

The following analysis holds for all k instants in time, hence we drop the argument k. The DOA measurement can be represented by a unit vector pointing from Agent B to Agent A. This vector is defined by azimuth and elevation angles θ and ϕ referenced to the local INS frame B_2, and its coordinates in the frame B_2 are given by:

$$\hat{\boldsymbol{q}}(\theta,\phi) = [\hat{q}_1, \hat{q}_2, \hat{q}_3] = [\cos\theta\cos\phi, \sin\theta\cos\phi, \sin\phi]^\top \tag{6}$$

Define $\bar{q} \doteq \|\boldsymbol{p}_{\boldsymbol{A}}^{\boldsymbol{B_2}} - \boldsymbol{p}_{\boldsymbol{B}}^{\boldsymbol{B_2}}\|$ as the Euclidean distance between Agent A and Agent B (which is not available to either agent). Scaling to obtain the unit vector $\hat{\boldsymbol{q}}$ gives

$$\hat{\boldsymbol{q}}(\theta,\phi) = \frac{1}{\bar{q}}\left[x_A - x_B,\quad y_A - y_B,\quad z_A - z_B\right]^\top \tag{7}$$

Applying equation (4) yields:

$$\begin{bmatrix}\hat{q}_1\\ \hat{q}_2\\ \hat{q}_3\end{bmatrix} = \frac{1}{\bar{q}}\begin{bmatrix}r_{11}u_A + r_{12}v_A + r_{13}w_A + t_1 - x_B\\ r_{21}u_A + r_{22}v_A + r_{23}w_A + t_2 - y_B\\ r_{31}u_A + r_{32}v_A + r_{33}w_A + t_3 - z_B\end{bmatrix} \quad (8)$$

The left hand vector is calculated directly from DOA measurements. Cross-multiplying entries 1 and 3 of both vectors eliminates the unknown $\bar{q}$, and rearranging yields:

$$\begin{aligned}&(u_A\hat{q}_3)r_{11} + (v_A\hat{q}_3)r_{12} + (w_A\hat{q}_3)r_{13} - (u_A\hat{q}_1)r_{31}\\ &- (v_A\hat{q}_1)r_{32} - (w_A\hat{q}_1)r_{33} + (\hat{q}_3)t_1 - (\hat{q}_1)t_3 \quad (9)\\ &= (\hat{q}_3)x_B - (\hat{q}_1)z_B\end{aligned}$$

Similarly, from the second and third entries in (8)

$$\begin{aligned}&(u_A\hat{q}_3)r_{21} + (v_A\hat{q}_3)r_{22} + (w_A\hat{q}_3)r_{23} - (u_A\hat{q}_2)r_{31}\\ &- (v_A\hat{q}_2)r_{32} - (w_A\hat{q}_2)r_{33} + (\hat{q}_3)t_2 - (\hat{q}_2)t_3 \quad (10)\\ &= (\hat{q}_3)y_B - (\hat{q}_2)z_B\end{aligned}$$

Notice that both equations (9) *and* (10) *are linear in the unknown r_{ij} and t_i terms.* Given a series of K DOA measurements (each giving $\phi(k), \theta(k)$), (9) and (10) can then be used to construct the following system of linear equations:

$$\boldsymbol{A}\boldsymbol{\Psi} = \boldsymbol{b}, \quad \boldsymbol{A} \in \mathbb{R}^{2K\times 12} \quad (11)$$

where $\boldsymbol{A}$, $\boldsymbol{b}$ are completely known, containing $\theta(k)$, $\phi(k)$, $\boldsymbol{p}_{\boldsymbol{A}}^{\boldsymbol{A_1}}$ and $\boldsymbol{p}_{\boldsymbol{B}}^{\boldsymbol{B_2}}$. The 12-vector of unknowns $\boldsymbol{\Psi}$ is defined as:

$$\boldsymbol{\Psi} = [r_{11}\ r_{12}\ r_{13}\ \ldots\ r_{31}\ r_{32}\ r_{33}\ t_1\ t_2\ t_3]^\top \quad (12)$$

Entry-wise definitions of $\boldsymbol{A}$ and $\boldsymbol{b}$ are provided in an extended version of this paper [22]. These entries of $\boldsymbol{\Psi}$ can be used to reconstruct the trajectory of Agent B in the global frame using (5), and therefore solving (11) for $\boldsymbol{\Psi}$ constitutes as a solution to the localisation problem. In the noiseless case, if $K \geq 6$ and $\boldsymbol{A}$ is of full column rank, equation (11) will be solvable.

B. *Example of LS method in noiseless case*

We demonstrate the linear system method using trajectories performed by aircraft operated by the Australian Defence Science and Technology Group. Positions of both Agent A and B within the global frame and Agent B within the INS frame were measured by on-board instruments, whereas we generated a set of *calculated* DOA values using the above recorded real measurements.

These trajectories are plotted in Figure 2. We will make additional use of this trajectory pair in the noisy measurement case presented in Section IV, and in the maximum likelihood estimation refinement of the noisy case localisation result in Section V. Extensive Monte Carlo simulations demonstrating localisation for a large number of realistic[5] flight trajectories are left to the noisy measurement case.

The quantities $\boldsymbol{R}_{\boldsymbol{A_1}}^{\boldsymbol{B_2}}$ and $\boldsymbol{t}_{\boldsymbol{A_1}}^{\boldsymbol{B_2}}$, and the DOA measurements are tabulated in the extended version of this paper [22]. Using (11), $\boldsymbol{R}_{\boldsymbol{A_1}}^{\boldsymbol{B_2}}$ and $\boldsymbol{t}_{\boldsymbol{A_1}}^{\boldsymbol{B_2}}$ were obtained exactly for the given flight trajectories; the solution is the green line in Fig. 2.

[5] By realistic, we mean that the distance separation between successive measurements is consistent with UAV flight speeds and ensures the UAV does not exceed an upper bound on the turn/climb rate. Further detail is provided in the extended version of this paper [22].

IV. Semidefinite Programming Method

This section presents a semidefinite programming (SDP) method for localisation, extending from the linear system (LS) approach presented in Section III. This method reduces the minimum required number of DOA measurements to obtain a unique solution, and is more robust than LS in terms of DOA measurement noise and unsuitable trajectories are reduced. Results from this section will serve as an initialisation of our localisation method, which will be optimised using maximum likelihood estimation in Section V.

Rank-relaxed SDP is used to incorporate the quadratic constraints on certain entries of $\boldsymbol{\Psi}$ arising from the properties of rotation matrices. The inclusion of rotation matrix constraints in SDP problems has been used previously to jointly estimate the attitude and spin-rate of a satellite [23], and in camera pose estimation using SFM techniques when directional measurements are made to multiple points simultaneously [24]. We now apply this technique in a novel context to achieve INS alignment of Agent B, sufficient for its localisation. Finally, the Orthogonal Procrustes algorithm (O) is used to compensate for the rank relaxation of the SDP.

A. *Quadratic constraints on entries of $\boldsymbol{\Psi}$*

Rank-relaxed semidefinite programming (in the presence of inexact or noise contaminated data) benefits from the inclusion of quadratic constraint equations. We now identify 21 quadratic and linearly independent constraint equations on entries of $\boldsymbol{R}_{\boldsymbol{A_1}}^{\boldsymbol{B_2}}$, which all appear in $\boldsymbol{\Psi}$ in (12). Recall the orthogonality property of rotation matrices; by computing each entry of $\boldsymbol{R}_{\boldsymbol{A_1}}^{\boldsymbol{B_2}}{\boldsymbol{R}_{\boldsymbol{A_1}}^{\boldsymbol{B_2}}}^\top$ and setting these equal to entries of $\boldsymbol{I_3}$, and denoting the i^{th} entry of $\boldsymbol{\Psi}$ as ψ_i, we define constraints:

$$C_i = \psi_{3i-2}^2 + \psi_{3i-1}^2 + \psi_{3i}^2 - 1 = 0, \quad i = 1, 2, 3 \quad (13a)$$
$$C_4 = \psi_1\psi_4 + \psi_2\psi_5 + \psi_3\psi_6 = 0 \quad (13b)$$
$$C_5 = \psi_1\psi_7 + \psi_2\psi_8 + \psi_3\psi_9 = 0 \quad (13c)$$
$$C_6 = \psi_4\psi_7 + \psi_5\psi_8 + \psi_6\psi_9 = 0 \quad (13d)$$

To simplify notation we call $C_{j:k}$ the set of constraints C_i for $i = j, .., k$. Similarly, by computing each entry of ${\boldsymbol{R}_{\boldsymbol{A_1}}^{\boldsymbol{B_2}}}^\top\boldsymbol{R}_{\boldsymbol{A_1}}^{\boldsymbol{B_2}}$ and setting these equal to $\boldsymbol{I_3}$, we define constraints $C_{7:12}$, which are omitted due to space limitations, and notice that the sets $C_{1:6}$ and $C_{7:12}$ are clearly equivalent.

Further constraints are required to ensure $\det(\boldsymbol{R}_{\boldsymbol{A_1}}^{\boldsymbol{B_2}}) = 1$. Cramer's formula states that ${\boldsymbol{R}_{\boldsymbol{A_1}}^{\boldsymbol{B_2}}}^{-1} = \mathrm{adj}(\boldsymbol{R}_{\boldsymbol{A_1}}^{\boldsymbol{B_2}})/\det(\boldsymbol{R}_{\boldsymbol{A_1}}^{\boldsymbol{B_2}})$, where $\mathrm{adj}(\boldsymbol{R}_{\boldsymbol{A_1}}^{\boldsymbol{B_2}})$ denotes the adjugate matrix of $\boldsymbol{R}_{\boldsymbol{A_1}}^{\boldsymbol{B_2}}$. Orthogonality of $\boldsymbol{R}_{\boldsymbol{A_1}}^{\boldsymbol{B_2}}$ implies $\boldsymbol{R}_{\boldsymbol{A_1}}^{\boldsymbol{B_2}} = \mathrm{adj}(\boldsymbol{R}_{\boldsymbol{A_1}}^{\boldsymbol{B_2}})^\top$. By computing entries of the first column of $\boldsymbol{Z} = \boldsymbol{R}_{\boldsymbol{A_1}}^{\boldsymbol{B_2}} - \mathrm{adj}(\boldsymbol{R}_{\boldsymbol{A_1}}^{\boldsymbol{B_2}})^\top$ and setting these equal to 0, we define constraints $C_{13:15}$:

$$C_{13} = \psi_1 - (\psi_5\psi_9 - \psi_6\psi_8) = 0 \quad (14a)$$
$$C_{14} = \psi_4 - (\psi_3\psi_8 - \psi_2\psi_9) = 0 \quad (14b)$$
$$C_{15} = \psi_7 - (\psi_2\psi_6 - \psi_3\psi_5) = 0 \quad (14c)$$

Similarly, by computing the entries of the second and third columns of $\boldsymbol{Z}$ and setting these equal to 0, we define constraints $C_{16:18}$ and $C_{19:21}$ respectively. Due to space limitations, we omit presenting them. The complete set $C_{1:21} \doteq C_\Psi$

constrains $\boldsymbol{R_{A_1}^{B_2}}$ to be a rotation matrix. The set of constraints is not an independent set, e.g. $\boldsymbol{C_{1:6}}$ is equivalent to $\boldsymbol{C_{7:12}}$. The benefits of the inclusion of dependent constraints is discussed further in Section IV-C.

Due to these additional relations, localisation requires azimuth and elevation measurements at a minimum of 4 instants only ($K = 4$), as opposed to 6 instants required in Section III.

B. Formulation of the Semidefinite Program

The goal of the semidefinite program is to obtain:

$$\underset{\boldsymbol{\Psi}}{\operatorname{argmin}} ||\boldsymbol{A\Psi} - \boldsymbol{b}|| \tag{15}$$

subject to C_Ψ. Equivalently, we seek $\operatorname{argmin}_\Psi ||\boldsymbol{A\Psi} - \boldsymbol{b}||^2$ subject to C_Ψ. We define the inner product of two matrices $\boldsymbol{U}$ and $\boldsymbol{V}$ as $\langle \boldsymbol{U}, \boldsymbol{V} \rangle = \text{trace}(\boldsymbol{U}\boldsymbol{V}^\top)$. One obtains

$$||\boldsymbol{A\Psi} - \boldsymbol{b}||^2 = \langle \boldsymbol{P}, \boldsymbol{X} \rangle \tag{16}$$

where $\boldsymbol{P} = \begin{bmatrix}\boldsymbol{A} & \boldsymbol{b}\end{bmatrix}^\top \begin{bmatrix}\boldsymbol{A} & \boldsymbol{b}\end{bmatrix}$ and $\boldsymbol{X} = [\boldsymbol{\Psi}^\top \ -1]^\top [\boldsymbol{\Psi}^\top \ -1]$ and $\boldsymbol{X}$ is a rank 1 positive-semidefinite matrix[6]. The constraints C_Ψ can also be expressed in inner product form. For $i = 1, ..., 21$, $C_i = 0$ is equivalent to $\langle \boldsymbol{Q_i}, \boldsymbol{X} \rangle = 0$ for some easily determined $\boldsymbol{Q_i}$. Solving for $\boldsymbol{\Psi}$ in (15) is therefore equivalent to solving for:

$$\underset{\Psi}{\operatorname{argmin}} \langle \boldsymbol{P}, \boldsymbol{X} \rangle \tag{17}$$

$$\boldsymbol{X} \geq 0 \tag{18}$$

$$\text{rank}(\boldsymbol{X}) = 1 \tag{19}$$

$$\boldsymbol{X_{13,13}} = 1 \tag{20}$$

$$\langle \boldsymbol{Q_i}, \boldsymbol{X} \rangle = 0 \qquad i = 1, ..., 21 \tag{21}$$

C. Rank Relaxation of Semidefinite Program

This semidefinite program is a reformulation of a quadratically constrained quadratic program (QCQP). Computationally speaking, QCQP problems are generally NP-hard. A close approximation to the true solution can be obtained in polynomial time if the rank 1 constraint on $\boldsymbol{X}$, i.e. (22), is relaxed. A full explanation of semidefinite relaxation, and discussion on its applicability can be found in [25]. This relaxation significantly increases the dimension of the SDP solver's codomain. A notable consequence is that dependent constraints which are linearly independent over $\mathbb{R}$ within $\boldsymbol{C_\Psi}$, such as sets $\boldsymbol{C_{1:6}}$ and $\boldsymbol{C_{7:12}}$, cease to be redundant when expressed as in (21). Hypothesis testing using extensive simulations confirmed with confidence above 95% that inclusion of quadratically dependent constraints improves the localisation accuracy.

The solution $\boldsymbol{X}$ obtained through rank-relaxed SDP is typically not a rank 1 matrix when DOA measurements are noisy. However the largest singular value of $\boldsymbol{X}$ is generally multiple orders of magnitude greater than the second largest singular value. A rank 1 approximation to $\boldsymbol{X}$, which we call $\boldsymbol{\hat{X}}$, is obtained by evaluating the singular value decomposition of $\boldsymbol{X}$, then setting all singular values except the largest equal to zero. From $\boldsymbol{\hat{X}}$, one can then use the definition of $\boldsymbol{X}$ to obtain the approximation of $\boldsymbol{\Psi}$, which we will call $\boldsymbol{\hat{\Psi}}$. Entries $\hat{\psi}_i$ for $i = 10, 11, 12$ can be used immediately to construct an estimate for $\boldsymbol{t_{A_1}^{B_2}}$, which we will call $\boldsymbol{\bar{t}}$. Entries $\hat{\psi}_i$ for $i = 1, ..., 9$ will be used to construct an intermediate approximation of $\boldsymbol{R_{A_1}^{B_2}}$, which we call $\boldsymbol{\widehat{R}}$, and which we will refine further.

[6]All matrices $\boldsymbol{M}$ which can be expressed in the form of $\boldsymbol{M} = \boldsymbol{v}^\top \boldsymbol{v}$ where $\boldsymbol{v}$ is a row vector are positive-semidefinite matrices.

D. Orthogonal Procrustes Algorithm

Due to the relaxation of the rank constraint (19) on $\boldsymbol{X}$, it is no longer guaranteed that entries of $\boldsymbol{\hat{\Psi}}$ strictly satisfy the set of constraints C_Ψ. Specifically, $\boldsymbol{\widehat{R}}$ may not be a rotation matrix. The Orthogonal Procrustes algorithm is a commonly used tool to determine the closest orthogonal matrix (denoted $\boldsymbol{\overline{R}}$) to a given matrix, $\boldsymbol{\widehat{R}}$. This is given by $\boldsymbol{\overline{R}} = \operatorname{argmin}_{\boldsymbol{\Omega}} ||\boldsymbol{\Omega} - \boldsymbol{\widehat{R}}||_F$, subject to $\boldsymbol{\Omega\Omega}^\top = I$, where $||.||_F$ is the Frobenius norm.

When noise is high, the above method occasionally returns $\boldsymbol{\overline{R}}$ such that $\det(\boldsymbol{\overline{R}}) = -1$. In this case, we employ a special case of the Orthogonal Procrustes algorithm [26] to ensure we obtain rotation matrices and avoid reflections by flipping the last column in one of the unitary matrix factors of the singular value decomposition.

The matrix $\boldsymbol{\overline{R}}$ and vector $\boldsymbol{\bar{t}}$ are the final estimates of $\boldsymbol{R_{A_1}^{B_2}}$ and $\boldsymbol{t_{A_1}^{B_2}}$ using semidefinite programming and the Orthogonal Procrustes algorithm. The estimate of Agent B's position in the global frame is $\overline{\boldsymbol{p_B^{A_1}}} = \boldsymbol{\overline{R}}^\top (\boldsymbol{p_B^{B_2}} - \boldsymbol{\bar{t}})$.

For convenience, we use SDP+O to refer to the process of solving a rank-relaxed semidefinite program, and then applying the Orthogonal Procrustes algorithm to the result.

E. Example of SDP+O method with noisy DOA measurements

In this subsection, we apply the SDP+O method to perform localisation in a noisy DOA measurement case using the real trajectory example from Section III. A popular practice for performing DOA measurements from Agent B towards Agent A is to use fixed RF-antennas and/or optical sensors on board Agent B's airframe. The horizontal RF antenna typically has a larger aperture (generally around 4 times, owing to the physical layout of a fixed-wing UAV) than the vertical RF antenna. As a result, errors in azimuth and elevation measurements, referenced to the body-fixed frame B_4, are modelled by independent zero-mean Gaussian distributed variables with different standard deviations, denoted σ_Θ and σ_Φ.

Strictly speaking, physical sensors return azimuth and elevation measurements in the interval $[0°, 360°)$, which means that each noise is expected to follow a von Mises distribution, which generalises a Gaussian distribution to a circle [27]. In our case, we approximate the von Mises distribution by a Gaussian distribution because noise is sufficiently small. In this example we assume body-fixed frame azimuth and elevation measurement errors have standard deviations of $\sigma_\Theta = 0.5°$ and $\sigma_\Phi = 2°$.

Samples of Gaussian error with these standard deviations were added to body-fixed frame (B_4) elevation and azimuth measurements calculated as described in Section III. These were converted to DOA measurements referenced to the INS

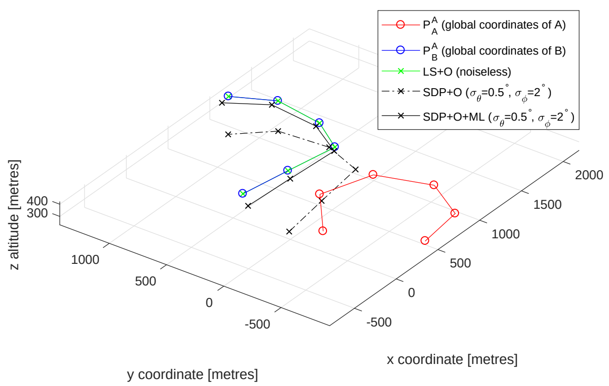

Fig. 2. Recovery of global coordinates of Agent B for recorded trajectories. Errors are $\sigma_\theta = 0.5^\circ$ and $\sigma_\phi = 2^\circ$ with respect to body fixed frame for the DOA measurements

frame B_3. The SDP+O algorithm was used to obtain $\overline{\boldsymbol{R}}$ and $\overline{\boldsymbol{t}}$ using the agents' position coordinates in their respective navigation frames and the noisy DOA values. The reconstructed trajectory $\overline{\boldsymbol{p}_{\boldsymbol{B}}^{\boldsymbol{A_1}}}$ is plotted in Figure 2 with the dotted black line. Position data of the reconstructed trajectory $\overline{\boldsymbol{p}_{\boldsymbol{B}}^{\boldsymbol{A_1}}}$ are tabulated in [22].

Remark 1. *The accuracy of the SDP+O solution in the noiseless case was observed to deteriorate when entries in the true translation vector (t_i for $i = 1, 2, 3$) are large. This is due to a form of inherent regularisation in the SDP solver Yalmip [28]. When the approximate magnitude of the norm $||\boldsymbol{t}_{\boldsymbol{A_1}}^{\boldsymbol{B_2}}||$ is known, one approach is to introduce a scaling coefficient before entries t_i for $i = 1, 2, 3$ in equations (9) and (10) equal to the approximate norm of $||\boldsymbol{t}_{\boldsymbol{A_1}}^{\boldsymbol{B_2}}||$.*

In [22], we discuss a controlled shifting algorithm which may be applied if an approximation of $\boldsymbol{t}_{\boldsymbol{A_1}}^{\boldsymbol{B_2}}$ is known a priori.

V. Maximum Likelihood Estimation

This section presents a maximum likelihood estimation (ML) method to optimise estimates $\overline{\boldsymbol{R}}$ and $\overline{\boldsymbol{t}}$ which were obtained using the SDP+O algorithm. The MLE refinement uses the DOA measurements expressed with respect to the body-fixed frame B_4, and the known values for σ_Θ and σ_Φ describing the distribution of DOA errors. A non-linear log-likelihood function for DOA measurement error is derived, and because the minimum of the function cannot be found analytically, we employ an iterative gradient descent approach.

A. *Likelihood Function Derivation*

In this section, DOA values are always expressed with respect to the body-fixed frame of Agent B (B_4) to exploit the independence of azimuth and elevation measurement errors. This is a change from Sections III and IV, in which DOA measurements were generally expressed with respect to the local INS frame B_2. The transformation between coordinate frames B_2 and B_4 is known to Agent B.

Suppose body-fixed frame measurements of azimuth and elevation $\Theta(k)$ and $\Phi(k)$ are contaminated by zero mean Gaussian noise as follows:

- $\widetilde{\Theta}(k) = \Theta(k) + \xi_\Theta, \quad \xi_\Theta \sim N(0, {\sigma_\Theta}^2)$
- $\widetilde{\Phi}(k) = \Phi(k) + \xi_\Phi, \quad \xi_\Phi \sim N(0, {\sigma_\Phi}^2)$

To calculate noiseless azimuth and elevation measurements, an expression must be derived for the position of Agent A in Agent B's body-fixed frame B_4. Observe that

$$\overline{\boldsymbol{p}_{\boldsymbol{A}}^{\boldsymbol{B4}}}(k) = \boldsymbol{R}_{\boldsymbol{B_2}}^{\boldsymbol{B_4}}(k)(\boldsymbol{R}_{\boldsymbol{A_1}}^{\boldsymbol{B_2}}\boldsymbol{p}_{\boldsymbol{A}}^{\boldsymbol{A_1}}(k) + \boldsymbol{t}_{\boldsymbol{A_1}}^{\boldsymbol{B_2}}) + \boldsymbol{t}_{\boldsymbol{B_2}}^{\boldsymbol{B_4}}(k) \tag{22}$$

To help distinguish coordinate reconstructions based on estimates of $\overline{\boldsymbol{R}}$ and $\overline{\boldsymbol{t}}$ from true coordinates, reconstructed positions will be explicitly expressed as functions of $\overline{\boldsymbol{R}}$ and $\overline{\boldsymbol{t}}$:

$$\overline{\boldsymbol{p}_{\boldsymbol{A}}^{\boldsymbol{B4}}}(k, \overline{\boldsymbol{R}}, \overline{\boldsymbol{t}}) = \boldsymbol{R}_{\boldsymbol{B_2}}^{\boldsymbol{B_4}}(k)(\overline{\boldsymbol{R}}\boldsymbol{p}_{\boldsymbol{A}}^{\boldsymbol{A_1}}(k) + \overline{\boldsymbol{t}}) + \boldsymbol{t}_{\boldsymbol{B_2}}^{\boldsymbol{B_4}}(k) \tag{23}$$

By definition of azimuth and elevation in Section II:

$$\theta_{B_4}(k, \overline{\boldsymbol{R}}, \overline{\boldsymbol{t}}) = \arcsin\left(\frac{\overline{\boldsymbol{p}_{\boldsymbol{A}}^{\boldsymbol{B4}}}(k, \overline{\boldsymbol{R}}, \overline{\boldsymbol{t}})_z}{||\overline{\boldsymbol{p}_{\boldsymbol{A}}^{\boldsymbol{B4}}}(k, \overline{\boldsymbol{R}}, \overline{\boldsymbol{t}})||}\right) \tag{24}$$

$$\phi_{B_4}(k, \overline{\boldsymbol{R}}, \overline{\boldsymbol{t}}) = \text{atan2}\Big(\overline{\boldsymbol{p}_{\boldsymbol{A}}^{\boldsymbol{B4}}}(k, \overline{\boldsymbol{R}}, \overline{\boldsymbol{t}})_y \, , \, \overline{\boldsymbol{p}_{\boldsymbol{A}}^{\boldsymbol{B4}}}(k, \overline{\boldsymbol{R}}, \overline{\boldsymbol{t}})_x\Big) \tag{25}$$

where $\overline{\boldsymbol{p}_{\boldsymbol{A}}^{\boldsymbol{B4}}} = [\overline{\boldsymbol{p}_{\boldsymbol{A}}^{\boldsymbol{B4}}}_x, \overline{\boldsymbol{p}_{\boldsymbol{A}}^{\boldsymbol{B4}}}_y, \overline{\boldsymbol{p}_{\boldsymbol{A}}^{\boldsymbol{B4}}}_z]^\top$. The likelihood function for the set of DOA measurements is defined as follows:

$$\begin{aligned}
&\boldsymbol{\mathcal{L}}(\boldsymbol{p}_{\boldsymbol{A}}^{\boldsymbol{A_1}}, \boldsymbol{p}_{\boldsymbol{B}}^{\boldsymbol{B_2}} | \overline{\boldsymbol{R}}, \overline{\boldsymbol{t}}) \\
&= \frac{1}{\sigma_\Theta\sqrt{2\pi}} \prod_{k=1}^{K} \exp\Big[-\frac{(\widetilde{\theta}_{B_4}(k) - \theta_{B_4}(k, \overline{\boldsymbol{R}}, \overline{\boldsymbol{t}}))^2}{2\sigma_\Theta^2}\Big] \\
&\times \frac{1}{\sigma_\Phi\sqrt{2\pi}} \prod_{k=1}^{K} \exp\Big[-\frac{(\widetilde{\phi}_{B_4}(k) - \phi_{B_4}(k, \overline{\boldsymbol{R}}, \overline{\boldsymbol{t}}))^2}{2\sigma_\Phi^2}\Big]
\end{aligned} \tag{26}$$

It can be shown that maximising $\boldsymbol{\mathcal{L}}(\boldsymbol{p}_{\boldsymbol{A}}^{\boldsymbol{A_1}}, \boldsymbol{p}_{\boldsymbol{B}}^{\boldsymbol{B_2}} | \overline{\boldsymbol{R}}, \overline{\boldsymbol{t}})$ is equivalent to minimising

$$\sum_{k=1}^{K}\Big[\frac{(\widetilde{\theta}_{B_4}(k) - \theta_{B_4}(k, \overline{\boldsymbol{R}}, \overline{\boldsymbol{t}}))^2}{2\sigma_\Theta^2} + \frac{(\widetilde{\phi}_{B_4}(k) - \phi_{B_4}(k, \overline{\boldsymbol{R}}, \overline{\boldsymbol{t}}))^2}{2\sigma_\Phi^2}\Big] \tag{27}$$

B. *Optimisation using gradient descent*

Possible parametrisations for the rotation matrix $\overline{\boldsymbol{R}}$ include Euler angles, quaternion representation and Rodrigues rotation formula. In this paper we parametrise $\overline{\boldsymbol{R}}$ by a 3-vector of Euler angles, and $\overline{\boldsymbol{t}}$ is a 3-vector. This defines a mapping from $\mathbb{R}^6 \to \overline{\boldsymbol{R}}, \overline{\boldsymbol{t}}$, and the gradient of (27) can be expressed as a vector in $\mathbb{R}^6$. The log-likelihood function is non-linear with respect to this $\mathbb{R}^6$ parametrisation of $\overline{\boldsymbol{R}}$ and $\overline{\boldsymbol{t}}$. As a result, this function may be non-convex, meaning the equation $\mathcal{D}\log\mathcal{L} = 0$ may have multiple solutions, with only one of these being the global minimum. A gradient descent algorithm is therefore initialised using the result of the SDP+O method, and is used to converge towards a local minimum, which it is hoped will be the global minimum or close to it. In our investigations, we employed a back-tracking line search algorithm discussed in [29]. External solvers such as Yalmip using second-order methods may yield faster convergence than a hard-coded approach.

C. Example of ML refinement of SDP+O solution

In this subsection, we demonstrate the benefits of maximum likelihood estimation. ML was performed using the real flight trajectory data presented in Section III. The resulting reconstructed trajectory $\overline{\boldsymbol{p}_{\boldsymbol{A}}^{\boldsymbol{B_2}}}$ is presented in Figure 2 as the solid black line, and its coordinates are tabulated in [22]. Additionally, in this section we present the decrease and convergence in the value of frame rotation error and reconstructed position error[7] over successive iterations of the gradient descent algorithm in Figures 3a and 3b.

The error in INS frame rotation is reduced by over 60%, and the reconstructed position error of Agent B is reduced by over 70% by iterating the gradient descent algorithm. This represents a significant gain with respect to the SDP+O estimate, which served as the initialisation point of the gradient descent. Monte Carlo simulations covering a large set of trajectories are presented in Section VI.

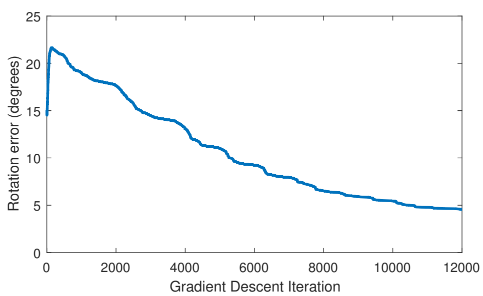

(a) Rotation error in degrees

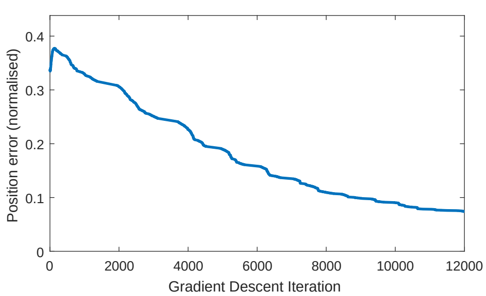

(b) Reconstructed position error

Fig. 3. Improvement in rotation and reconstructed position error using ML for real trajectory pair

VI. Simulation Results

In this section, we use extensive simulations of realistic[8] flight trajectories to evaluate the effects of errors in body-fixed frame azimuth and elevation measurements, and then discuss trajectories which make localisation difficult.

In the preliminary conference paper [21] found that the LS+O method collapsed when small amounts of noise were introduced to DOA measurements, whereas rotation error increased linearly with respect to DOA measurement noise when using the SDP+O method. The SDP+O method is the superior method, and there is no reason to employ LS+O.

[7]Metrics are defined in the sequel, see Section VI-A below.

[8]These trajectories satisfy a set of assumptions detailed in [22].

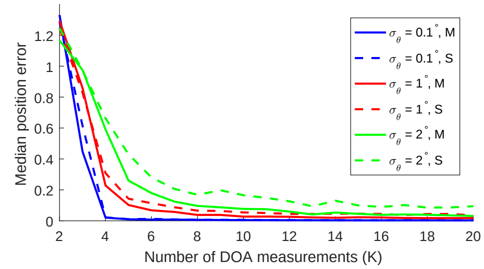

Fig. 4. Median $error(\overline{\boldsymbol{p}_{\boldsymbol{B}}^{\boldsymbol{A_1}}})$ vs. number of DOA measurements used to solve SDP+O (S) and SDP+O+ML (M) from $K = 2$ to $K = 20$.

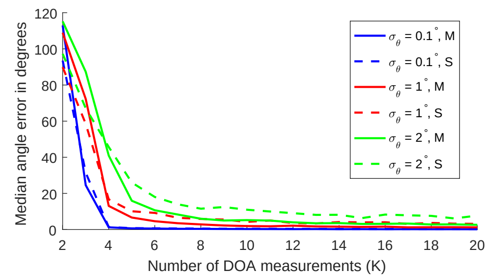

Fig. 5. Median $d(\overline{\boldsymbol{R}}, \boldsymbol{R}_{\boldsymbol{A}}^{\boldsymbol{B}})$ vs. number of DOA measurements used to solve SDP+O (S) and SDP+O+ML (M) from $K = 2$ to $K = 20$

A. Metrics for error in $\overline{\boldsymbol{R}}$ and $\overline{\boldsymbol{t}}$

This paper uses the geodesic metric for rotation [30]. All sequences of rotations in three dimensions can be expressed as one rotation about a single axis [31]. The geodesic metric on $SO(3)$ defined by

$$d(\boldsymbol{R_1}, \boldsymbol{R_2}) = \arccos\left(\frac{\operatorname{tr}(\boldsymbol{R_1}^\top \boldsymbol{R_2}) - 1}{2}\right) \tag{28}$$

is the magnitude of angle of rotation about this axis [32]. Where $\boldsymbol{R}_{\boldsymbol{A}}^{\boldsymbol{B}}$ is known, the error of rotation $\overline{\boldsymbol{R}}$ is defined as $d(\overline{\boldsymbol{R}}, \boldsymbol{R}_{\boldsymbol{A}}^{\boldsymbol{B}})$. Position error is defined as the average Euclidian distance between true global coordinates of Agent B, and estimated global coordinates over the K measurements taken, divided (to secure normalisation) by the average distance between aircraft.

$$error(\overline{\boldsymbol{p}_{\boldsymbol{B}}^{\boldsymbol{A_1}}}) = \frac{\sum_k ||\overline{\boldsymbol{p}_{\boldsymbol{B}}^{\boldsymbol{A_1}}}(k) - \boldsymbol{p}_{\boldsymbol{B}}^{\boldsymbol{A_1}}(k)||}{Kd} \tag{29}$$

where $\overline{\boldsymbol{p}_{\boldsymbol{B}}^{\boldsymbol{A_1}}}(k) = \overline{\boldsymbol{R}}^\top(\boldsymbol{p}_{\boldsymbol{B}}^{\boldsymbol{B_2}} - \overline{\boldsymbol{t}})$, and d represents the average distance between aircraft.

B. Monte Carlo Simulations using SDP+O and ML

In this subsection, we summarise the results of Monte Carlo simulations to evaluate the expected performance of the SDP+O method and the SDP+O+ML method.

Pairs of realistic trajectories for Agents A and B are generated in accordance with a series of assumptions related to real flight dynamics listed in the extended version of this paper [22]. To represent the drift in the INS of Agent B, rotations $\boldsymbol{R}_{\boldsymbol{A_1}}^{\boldsymbol{B_2}}$ were generated by independently sampling three Euler angles α, β, γ where $\alpha, \beta, \gamma \sim U(-\pi, \pi)$, and translations $\boldsymbol{t}_{\boldsymbol{A_1}}^{\boldsymbol{B_2}} = [t_1, t_2, t_3]^\top$ were generated by sampling entries $t_1, t_2, t_3 \sim U(-600, 600)$.

As discussed in Section IV-E, we assume the standard deviations of measurement error in the body-fixed frame B_4 satisfy $\sigma_\Phi = 4\sigma_\Theta$. We vary the DOA error by $\sigma_\Theta \in \{0.1^\circ, 1^\circ, 2^\circ\}$. Errors in the order of $\sigma_\Theta = 0.1^\circ$ are representative of an optical sensor, whereas the larger errors are representative of antenna-based (RF) measurements.

For each value of σ_Θ studied, and for each number of DOA measurements K from 2 to 20, we simulated 100 different realistic UAV trajectory pairs (Agent A and Agent B). For each trajectory pair, localisation was performed using the SDP+O method, and metrics $d(\overline{\boldsymbol{R}}, \boldsymbol{R}_{\boldsymbol{A}}^{\boldsymbol{B}})$ and $error(\overline{\boldsymbol{P}_{\boldsymbol{B}}^{\boldsymbol{A_1}}})$, were calculated. The ML method was then used to enhance the result of the SDP+O method, and the error metrics were re-calculated. After all simulations were completed, the median[9] values of $d(\overline{\boldsymbol{R}}, \boldsymbol{R}_{\boldsymbol{A}}^{\boldsymbol{B}})$ and $error(\overline{\boldsymbol{P}_{\boldsymbol{B}}^{\boldsymbol{A_1}}})$ for both the SDP+O and SDP+O+ML methods were calculated across each set 100 simulations. The results of the Monte Carlo simulations are plotted in Figures 4 and 5.

Median $d(\overline{\boldsymbol{R}}, \boldsymbol{R}_{\boldsymbol{A}}^{\boldsymbol{B}})$ and $error(\overline{\boldsymbol{P}_{\boldsymbol{B}}^{\boldsymbol{A_1}}})$ errors decrease significantly when 4 or more DOA measurements (K) are used. Both metrics show an asymptotic limit to performance across all three noise levels as the number of DOA measurements (K) increases. Median rotation error $d(\overline{\boldsymbol{R}}, \boldsymbol{R}_{\boldsymbol{A}}^{\boldsymbol{B}})$ and $error(\overline{\boldsymbol{p}_{\boldsymbol{B}}^{\boldsymbol{A_1}}})$ appear to exhibit similar asymptotic performance gain over the number of DOA measurements K up to 20.

C. Unsuitable trajectories for localisation

In this subsection we are motivated to identify trajectories of Agents A and B which may lead to multiple solutions for $\overline{\boldsymbol{R}}$ and $\bar{\boldsymbol{t}}$ in the noiseless case, and consequently unreliable solutions in the noisy case. We discuss three scenarios:

1) Agent A's motion is planar
2) The agents' trajectories produce equal DOA measurements with respect to Agent B's INS frame.
3) Agent A's trajectory is a point or straight line

The first scenario is an example of conditional unsuitability. When Agent A's motion is planar, matrix $\boldsymbol{A}$ in Eqn. (11) is rank deficient, and a unique solution cannot be obtained by solving Eqn. (11). In contrast, by introducing quadratic constraints through SDP, the correct solution is obtained.

The second and third scenarios are examples where the inability to discern a unique solutions is not because of an algorithmic deficiency, but rather because there is geometric ambiguity arising from unsuitable trajectories.

In the second scenario, DOA measurements expressed with respect to the local INS frame B_2 are equal at each time instant. This is illustrated by an example in Fig. 6. A similar problem is expected in the far field case, where the distance between Agents A and B is sufficiently large that DOA measurements become approximately equal despite each agent's trajectory remaining arbitrary. In these cases, multiple solutions exist for $\boldsymbol{t}_{\boldsymbol{A_1}}^{\boldsymbol{B_2}}$.

[9]For asymmetric distributions such as nonnegative errors (which may contain extreme outliers), the median is a superior measure of central tendency than the mean [33], [34].

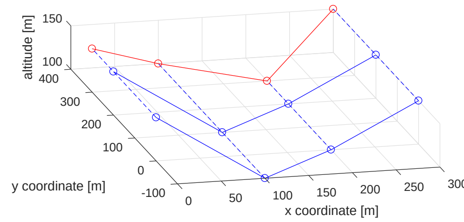

Fig. 6. Illustration of trajectory pairs leading to equal DOA measurements (disconnected blue lines) over K measurement instants. SDP+O+ML algorithm unable to discern distance from which Agent B (solid blue) observes Agent A (red).

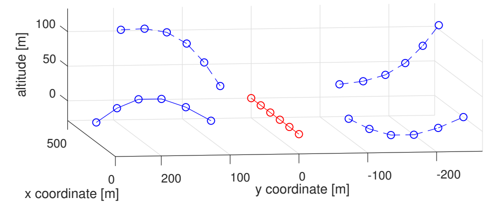

Fig. 7. Illustration of straight line motion of Agent A (red, trajectory given by $(x(t), y(t), z(t)) = (100t, 0, 0)$). Agent B (blue) observes Agent A through an unaligned INS frame. In this figure, the solid blue trajectory is the actual path of Agent B. However, each dotted blue line is also an admissible solution.

In the third scenario, Agent A's trajectory appears similar from multiple perspectives. As a consequence, the localisation process may be incapable of determining the direction from which DOA measurements were taken with respect to the global frame. For example, if Agent A follows a straight line, the same set of recorded DOA measurements may be achieved by viewing Agent A from any direction in a circle perpendicular to Agent A's motion and centred at Agent A's trajectory. This is illustrated in Figure 7.

VII. Three-Agent Extension and Beyond

This section explores a novel extension to the SDP+O+ML algorithm to localise two GPS-denied agents efficiently. Trivially, each GPS-denied aircraft could measure DOA of the GPS-equipped agent's broadcast of its position, and use the SDP+O+ML algorithm independently of each other to estimate drift in their local frames. We are motivated to determine whether a *trilateral*[10] algorithm may be more resilient to DOA measurement error and/or unsuitable trajectories, and may perhaps require fewer DOA measurements from each aircraft than simply repeating the two-agent localisation algorithm with each GPS-denied agent. We introduce a GPS-denied Agent C, whose local INS frame has rotation and translation parameters $\boldsymbol{R}_{\boldsymbol{A_1}}^{\boldsymbol{C_2}}$ and $\boldsymbol{t}_{\boldsymbol{A_1}}^{\boldsymbol{C_2}}$ with respect to the global frame. We conclude this section by discussing the challenges involved in generalising our findings to arbitrary n-agent networks.

[10]In this section we relax the condition preventing GPS-denied agents from broadcasting signals

A. Measurement process in three-agent network

To describe measurements within a network of more than two agents, one minor notation change is required: DOA measurements made by Agent I towards Agent J will henceforth be expressed in the INS coordinate frame of Agent I as ($\theta^J_{I_2}$, $\phi^J_{I_2}$). At each time instant k in the discrete-time process:

- Agents A and B interact as per the two-agent case.
- Agent C receives the broadcast of Agent A's global coordinates, and measures this signal's DOA with respect to frame C_2, which we denote ($\theta^A_{C_2}$, $\phi^A_{C_2}$).
- Agent C broadcasts its position with respect to its INS frame $\boldsymbol{p}^{\boldsymbol{C_2}}_{\boldsymbol{C}}$, as well as the measurement ($\theta^A_{C_2}$, $\phi^A_{C_2}$) to Agent B, who also takes a DOA measurement towards Agent C. This measurement is denoted ($\theta^C_{B_2}$, $\phi^C_{B_2}$).

All DOA and position measurements are relayed to Agent B, who performs the localisation algorithm discussed below.

B. Forming system of linear equations in three-agent network

In Section III, the linear system $\boldsymbol{A\Psi} = \boldsymbol{b}$ was formed using relations stemming from the collinearity of the vector ($\boldsymbol{p}^{\boldsymbol{B_2}}_{\boldsymbol{A}} - \boldsymbol{p}^{\boldsymbol{B_2}}_{\boldsymbol{B}}$), and the vector in the direction of DOA measurement ($\theta^A_{B_2}$, $\phi^A_{B_2}$). We refer to this system of equations as $\boldsymbol{S_{AB}}$, where the subscript references the agents involved. A similar system $\boldsymbol{S_{AC}}$ can be constructed independently using Agent C's DOA measurements towards Agent A and $\boldsymbol{p}^{\boldsymbol{C_2}}_{\boldsymbol{C}}$.

In the three-agent network, Agent B also measures the DOA towards Agent C's broadcast, with respect to Agent B's local INS frame B_2. To exploit the collinearity of the vectorial representation of the DOA measurement ($\theta^C_{B_2}$, $\phi^C_{B_2}$) and ($\boldsymbol{p}^{\boldsymbol{B_2}}_{\boldsymbol{C}} - \boldsymbol{p}^{\boldsymbol{B_2}}_{\boldsymbol{B}}$), an expression for the position coordinate vector $\boldsymbol{p}^{\boldsymbol{B_2}}_{\boldsymbol{C}}$ is required. As achieved in equations (7) and (8) in Section III, this position may be expressed in terms of entries of $\boldsymbol{R}^{\boldsymbol{B_2}}_{\boldsymbol{C_2}}$ and $\boldsymbol{t}^{\boldsymbol{B_2}}_{\boldsymbol{C_2}}$, and the linear system $\boldsymbol{S_{BC}}$ may be defined similarly to $\boldsymbol{S_{AB}}$ in Section III. Systems $\boldsymbol{S_{AB}}$, $\boldsymbol{S_{AC}}$ and $\boldsymbol{S_{BC}}$ can be assembled, forming a large system of linear equations $\boldsymbol{S_{ABC}}$ with 36 scalar unknowns (9 rotation matrix entries and 3 translation vector entries per agent pair).

At each time instant k for $k = 1, ..., K$, two linear equations are obtained from each DOA measurement of ($\theta^A_{B_2}$, $\phi^A_{B_2}$), ($\theta^A_{C_2}$, $\phi^A_{C_2}$) and ($\theta^{C_2}_{B_2}$, $\phi^{C_2}_{B_2}$). As a result, 6 linear equations are obtained at each time instant. Performing the measurement process 6 times ($K = 6$) produces 36 linear equations. Generically, in the noiseless case, a unique solution therefore exists for $K = 6$ time instants. When using only the LS method, the three-agent localisation problem requires the same minimum number of time instants as solving two independent two-agent localisation problems concurrently, yet requires more DOA measurements than the sum of the number of measurements required in two separate two-agent localisation problems. However, quadratic relationships between $\boldsymbol{R}^{\boldsymbol{B_2}}_{\boldsymbol{A_1}}$, $\boldsymbol{t}^{\boldsymbol{B_2}}_{\boldsymbol{A_1}}$, $\boldsymbol{R}^{\boldsymbol{C_2}}_{\boldsymbol{A_1}}$, $\boldsymbol{t}^{\boldsymbol{C_2}}_{\boldsymbol{A_1}}$, $\boldsymbol{R}^{\boldsymbol{C_2}}_{\boldsymbol{B_2}}$ and $\boldsymbol{t}^{\boldsymbol{C_2}}_{\boldsymbol{B_2}}$ significantly reduce the required number of time instants (K) at which measurements occur.

C. Quadratic constraints in three-agent network and example

It is possible, using the rotational and translational relationships between the three frames, to obtain a total of 99 linearly independent quadratic constraints for a system of 36 unknown variables. Exact details are given in [22] for the interested reader, but omitted here for spatial considerations.

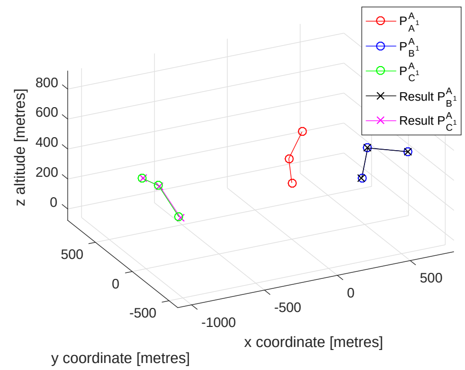

Fig. 8. Illustration of example of successful localisation within three-agent network in noiseless case for K = 3

Rank-relaxed semidefinite programming can be used to obtain solutions for each INS frame's rotation and translation with respect to the global frame, and the Orthogonal Procrustes algorithm can be applied to each individual resulting rotation matrix. This defines the three-agent SDP+O method.

To illustrate successful localisation in the three-agent case, realistic trajectories were defined for Agents A, B and C for $K = 3$ time instants. These are presented in Figure 8. Only Agents B and C were assigned random INS frame rotations and translations as prescribed in Section VI, and the three-agent SDP+O method was used to obtain estimates of $\boldsymbol{R}^{\boldsymbol{B_2}}_{\boldsymbol{A_1}}$, $\boldsymbol{t}^{\boldsymbol{B_2}}_{\boldsymbol{A_1}}$, $\boldsymbol{R}^{\boldsymbol{C_2}}_{\boldsymbol{A_1}}$ and $\boldsymbol{t}^{\boldsymbol{C_2}}_{\boldsymbol{A_1}}$. Each directional measurement consists of two scalar measurements, and hence a total of $3 \times 2 \times K = 18$ scalar measurements were obtained. Localisation was successful, which demonstrates that only 3 time instants ($K = 3$) are required for the three-agent SDP+O algorithm to obtain the exact solution in the noiseless case. Earlier, it was established that a minimum of 6 time instants were required to achieve a unique solution in the three-agent case using LS+O, and a minimum of 4 time instants were required to achieve a unique solution in the two-agent case using SDP+O. We have therefore demonstrated that a trilateral algorithm can achieve localisation of two GPS-denied agents in fewer measurement time instants than applying the bilateral algorithm twice independently. We note that this extension to three-agents is not applicable if the measurement graph is a tree because measurements are required between each pair of agents within the three-agent network.

D. Challenges in extension to n-agent networks

Advancing to arbitrary n-agent networks requires results on bearing rigidity of a graph. Though results exist when all agents share the same reference frame [35]–[37], there is no such result when, as in our problem, agents have different reference frames. We note that algebraic conditions for 3D bearing localisability based on the rank of generalised versions of the rigidity matrix have recently been identified in [25] and [23]. There is also the risk of an explosion in computational complexity due to a potentially exponential increase in the number of variables (entries of rotation matrices and translation vectors) that need to be determined. Further discussion can be found in [22].

VIII. Conclusion

This paper studied a cooperative localisation problem between a GPS-denied and a GPS-enabled UAV. A localisation algorithm was developed in two stages. We showed that a linear system of equations built from six or more measurements yielded the localisation solution for generic trajectories. The second stage considered the inclusion of quadratic constraints due to rotation matrix constraints. Rank relaxed semidefinite programming was used, and the solution adjusted using the Orthogonal Procrustes algorithm. This gave the algorithm greater resilience to noisy measurements and unsuitable trajectories. Maximum likelihood estimation was then used to improve the algorithm's results. Simulations were presented to illustrate the algorithm's performance. Finally, an approach was outlined to extend the two-agent solution to a three agent network in which only one agent has global localisation capacity. Future work may include implementation on aircraft to perform localisation in real time and validate our Monte Carlo analysis on measurement noise. We also hope to extend our trilateral algorithm to larger networks by establishing further theory on bearing rigidity when agents do not share a common reference frame.

References

[1] G. Balamurugan, J. Valarmathi, and V. Naidu, "Survey on UAV Navigation in GPS Denied Environments," in *Signal Processing, Communication, Power and Embedded System (SCOPES), 2016 International Conference on*. IEEE, 2016, pp. 198–204.

[2] H. Bai and R. W. Beard, "Relative Heading Estimation for Target Handoff in GPS-Denied Environments," in *American Control Conference (ACC), 2016*. IEEE, 2016, pp. 336–341.

[3] J. Morales, P. Roysdon, and Z. Kassas, "Signals of Opportunity Aided Inertial Navigation," in *Proceedings of ION GNSS Conference*, 2016, pp. 1492–1501.

[4] J. Morales and Z. M. Kassas, "Information fusion strategies for collaborative radio slam," in *2018 IEEE/ION Position, Location and Navigation Symposium (PLANS)*, April 2018, pp. 1445–1454.

[5] J. Morales and Z. Kassas, "A Low Communication Rate Distributed Inertial Navigation Architecture with Cellular Signal Aiding," in *2018 IEEE 87th Vehicular Technology Conference (VTC Spring)*. IEEE, 2018, pp. 1–6.

[6] ——, "Distributed Signals of Opportunity Aided Inertial Navigation with Intermittent Communication," in *2017 ION GNSS+ Conference*, 2017, pp. 2519–2530.

[7] A. N. Bishop, B. Fidan, B. D. O. Anderson, K. Dogancay, and P. N. Pathirana, "Optimality Analysis of Sensor-Target Geometries in Passive Localization: Part 1 - Bearing-Only Localization," in *Intelligent Sensors, Sensor Networks and Information*, Dec 2007, pp. 7–12.

[8] L. G. Taff, "Target Localization From Bearings-Only Observations," *IEEE Transactions on Aerospace and Electronic Systems*, vol. 33, no. 1, pp. 2–10, Jan 1997.

[9] O. Tekdas and V. Isler, "Sensor Placement for Triangulation-Based Localization," *IEEE Transactions on Automation Science and Engineering*, vol. 7, no. 3, pp. 681–685, July 2010.

[10] P. Batista, C. Silvestre, and P. Oliveira, "Navigation systems based on multiple bearing measurements," *IEEE Transactions on Aerospace and Electronic Systems*, vol. 51, no. 4, pp. 2887–2899, Oct 2015.

[11] K. Dogancay, "Self-Localization from Landmark Bearings using Pseudolinear Estimation Techniques," *IEEE Transactions on Aerospace and Electronic Systems*, vol. 50, no. 3, pp. 2361–2368, July 2014.

[12] Y. Duan, R. Ding, and H. Liu, "A Probabilistic Method of Bearing-only Localization by Using Omnidirectional Vision Signal Processing," in *Intelligent Information Hiding and Multimedia Signal Processing (IIH-MSP), 2012 Eighth International Conference on*, July 2012, pp. 285–288.

[13] P. Batista, C. Silvestre, and P. Oliveira, "Globally Exponentially Stable Filters for Source Localization and Navigation Aided by Direction Measurements," *Systems & Control Letters*, vol. 62, no. 11, pp. 1065 – 1072, 2013.

[14] H. Bayram, J. V. Hook, and V. Isler, "Gathering Bearing Data for Target Localization," *IEEE Robotics and Automation Letters*, vol. 1, no. 1, pp. 369–374, Jan 2016.

[15] M. Gavish and A. J. Weiss, "Performance Analysis of Bearing-Only Target Location Algorithms," *IEEE Transactions on Aerospace and Electronic Systems*, vol. 28, no. 3, pp. 817–828, Jul 1992.

[16] S. Sohn, B. Lee, J. Kim, and C. Kee, "Vision-Based Real-Time Target Localization for Single-Antenna GPS-Guided UAV," *IEEE Transactions on Aerospace and Electronic Systems*, vol. 44, no. 4, pp. 1391–1401, Oct 2008.

[17] J. Reis, P. Batista, P. Oliveira, and C. Silvestre, "Source Localization Based on Acoustic Single Direction Measurements," *IEEE Transactions on Aerospace and Electronic Systems*, pp. 1–1, 2018.

[18] J. J. Koenderink and A. J. van Doorn, "Affine Structure From Motion," *J. Opt. Soc. Am. A*, vol. 8, no. 2, pp. 377–385, Feb 1991.

[19] M. Ye, B. D. O. Anderson, and C. Yu, "Bearing-Only Measurement Self-Localization, Velocity Consensus and Formation Control," *IEEE Transactions on Aerospace and Electronic Systems*, vol. 53, no. 2, pp. 575–586, April 2017.

[20] L. Zhang, M. Ye, B. D. O. Anderson, P. Sarunic, and H. Hmam, "Cooperative localisation of uavs in a gps-denied environment using bearing measurements," in *2016 IEEE 55th Conference on Decision and Control (CDC)*, Dec 2016, pp. 4320–4326.

[21] J. S. Russell, M. Ye, B. D. Anderson, H. Hmam, and P. Sarunic, "Cooperative Localisation of a GPS-Denied UAV in 3-Dimensional Space Using Direction of Arrival Measurements," *IFAC-PapersOnLine*, vol. 50, no. 1, pp. 8019 – 8024, 2017, 20th IFAC World Congress.

[22] J. S. Russell, M. Ye, B. D. O. Anderson, H. Hmam, and P. Sarunic, "Cooperative Localisation of GPS-Denied UAVs using Direction of Arrival Measurements," 2018. [Online]. Available: http://arxiv.org/abs/1804.04317

[23] M. Pasquetti, G. Michieletto, S. Zhao, D. Zelazo, and A. Cenedese, "A Unified Dissertation on Bearing Rigidity Theory," *CoRR*, 2019.

[24] M. Arie-Nachimson, S. Z. Kovalsky, I. Kemelmacher-Shlizerman, A. Singer, and R. Basri, "Global Motion Estimation from Point Matches," in *Proceedings of the 2012 Second International Conference on 3D Imaging, Modeling, Processing, Visualization & Transmission*, 2012, pp. 81–88.

[25] F. Schiano and R. Tron, "The Dynamic Bearing Observability Matrix Nonlinear Observability and Estimation for Multi-Agent Systems," in *ICRA 2018 - IEEE International Conference on Robotics and Automation*. Brisbane, Australia: IEEE, May 2018, pp. 1–8.

[26] D. Eggert, A. Lorusso, and R. Fisher, "Estimating 3-D Rigid Body Transformations: A Comparison of Four Major Algorithms," *Machine Vision and Applications*, vol. 9, no. 5, pp. 272–290, Mar 1997.

[27] C. Forbes, M. Evans, N. Hastings, and B. Peacock, *Statistical Distributions*. John Wiley & Sons, 2011.

[28] J. Löfberg, "YALMIP : A Toolbox for Modeling and Optimization in MATLAB," in *In Proceedings of the CACSD Conference*, Taipei, Taiwan, 2004.

[29] P. S. Stanimirović and M. B. Miladinović, "Accelerated Gradient Descent Methods with Line Search," *Numerical Algorithms*, vol. 54, no. 4, pp. 503–520, 2010.

[30] D. Q. Huynh, "Metrics for 3D Rotations: Comparison and Analysis," *Journal of Mathematical Imaging and Vision*, vol. 35, no. 2, pp. 155–164, 2009.

[31] B. Palais, R. Palais, and S. Rodi, "A Disorienting Look at Euler's Theorem on the Axis of a Rotation," *American Mathematical Monthly*, vol. 116, no. 10, pp. 892–909, 2009.

[32] R. Tron, J. Thomas, G. Loianno, K. Daniilidis, and V. Kumar, "A Distributed Optimization Framework for Localization and Formation Control: Applications to Vision-Based Measurements," *IEEE Control Systems*, vol. 36, no. 4, pp. 22–44, Aug 2016.

[33] S. Boslaugh, *Statistics in a Nutshell: A Desktop Quick Reference*. O'Reilly Media, Inc., 2012.

[34] H. L. Harter, "The Method of Least Squares and Some Alternatives: Part II," *International Statistical Review*, vol. 42, no. 3, pp. 235–282, 1974.

[35] S. Zhao and D. Zelazo, "Bearing Rigidity and Almost Global Bearing-Only Formation Stabilization," *IEEE Transactions on Automatic Control*, vol. 61, no. 5, pp. 1255–1268, May 2016.
[36] D. Zelazo, A. Franchi, and P. R. Giordano, "Rigidity theory in se(2) for unscaled relative position estimation using only bearing measurements," *2014 European Control Conference (ECC)*, pp. 2703–2708, 2014.
[37] S. Zhao and D. Zelazo, "Localizability and Distributed Protocols for Bearing-Based Network Localization in Arbitrary Dimensions," *Automatica*, vol. 69, pp. 334 – 341, 2016.